Topological nodal line semimetals in the CaP₃ family of materials

Qiunan Xu,[1,2] Rui Yu,[3,*] Zhong Fang,[1,2] Xi Dai,[1,2] and Hongming Weng[1,2,†]

[1]*Beijing National Laboratory for Condensed Matter Physics, and Institute of Physics, Chinese Academy of Sciences, Beijing 100190, China*
[2]*Collaborative Innovation Center of Quantum Matter, Beijing 100190, China*
[3]*Department of Physics, Harbin Institute of Technology, Harbin 150001, China*

By using first-principles calculations and a $k \cdot p$ model analysis, we propose that the three-dimensional topological nodal line semimetal state can be realized in the CaP₃ family of materials, which includes CaP₃, CaAs₃, SrP₃, SrAs₃, and BaAs₃, when spin-orbit coupling (SOC) is ignored. The closed topological nodal line near the Fermi energy is protected by time reversal symmetry and spatial inversion symmetry. Moreover, drumheadlike two-dimensional surface states are also obtained on the c-direction surface of these materials. When SOC is included, the gaps open along the nodal line and these materials become strong topological insulators with Z_2 indices as (1; 010).

I. INTRODUCTION

The study of topological semimetals [1] has attracted broad interests from both the theoretical and the experimental communities in recent years. Generally speaking, topological semimetals are topologically stable since their Fermi surfaces enclose nontrivial band crossing points in crystal momentum space. Such band crossing points behave as the monopoles of a Berry flux [2,3], and bring a quantized Berry flux when passing through the surrounding enclosed Fermi surface [2,4]. This quantized number can be taken as the topological invariant to identify the band topology of the corresponding metals. Based on the degeneracy of the band crossing points and their distribution in the Brillouin zone (BZ), topological semimetals can classify into Dirac semimetals, Weyl semimetals, and nodal line semimetals. For Dirac semimetals, the band crossing points are fourfold degenerate, which can be seen as three-dimensional versions of graphene. This novel state has been theoretically proposed and experimentally confirmed in the Na₃Bi and Cd₃As₂ compounds [5–12]. For Weyl semimetals, the band crossing points are double degenerate, with definite chirality, and are located at an even number of discrete points in the BZ, which have been theoretically predicted [13–15] and very recently have been experimentally verified in the TaAs family of materials [16–21]. For topological nodal line semimetals [22,23], the band crossing points form closed loops instead of discrete points in the BZ. Now, many theoretically proposed materials for realizing these topological states have emerged, including Bernal graphite [24–26], Mackay-Terrones crystals [27], hyperhoneycomb lattices [28], Ca₃P₂ [29,30], LaN [31], Cu₃(Pd,Zn)N [32,33], the interpenetrated graphene network [34], (Tl,Pb)TaSe₂ [35,36], ZrSiS [37], perovskite iridates [38–41], CaAgX (X = P,As) [42], BaMX₃ (M = V, Nb, Ta; X = S, Se) [43], black phosphorus [44], calcium, strontium, and ytterbium [45]. It has been also proposed that a nodal line structure can be realized by considering the instabilities in a Weyl metal with transverse ordered spin-density waves (SDW$_{x,y}$) or charge-density waves

[46]. The intriguing expected properties characterizing topological nodal line semimetals include drumheadlike nearly flat surface states [27,32,33,47], unique Landau energy levels [48], long-range Coulomb interactions [49], special collective modes [50], and the opening of an important route to achieving high-temperature superconductivity [51–53].

In the present paper, based on first-principles calculations and a $k \cdot p$ model Hamiltonian analysis, we predict that the CaP₃ family of materials is another candidate for topological nodal line semimetals. The rest of the paper is organized as follows. In Sec. II, we present the crystal structure and the first-principles calculation methodology. Then we present the calculated bulk and surface electronic structures of the CaP₃ family of materials in Sec. III A. In Sec. III B, an effective $k \cdot p$ model is constructed and the nodal line structure and the surface states are studied from the $k \cdot p$ Hamiltonian. Conclusions are given at the end of this paper.

II. CRYSTAL STRUCTURE AND COMPUTATIONAL METHOD

The crystal structure of the CaP₃ families can be viewed as a list of two-dimensional (2D) infinite puckered polyanionic layers $_\infty^2[P_3]^{2-}$ [54] [see Fig. 1(b)] stacking along the b axis. The P layers form channels in the a-c direction and the cations are inserted into the channels, as shown in Fig. 1(d). The space group of CaP₃ and CaAs₃ is $P\bar{1}$, while SrP₃, SrAs₃, and BaAs₃ have a higher symmetry which is characterized by the space group $C2/m$. Moreover, lattice a is equivalent to c in the space group $C2/m$, but in $P\bar{1}$ it is not. The crystallographic data and the atomic coordinates for these materials are listed in Tables I and II. The primitive cell illustrated in Figs. 1(a) and 1(c) is used in the following calculation.

The first-principles calculations are performed by using the Vienna *ab initio* simulation package (VASP) based on the generalized gradient approximation (GGA) in the Perdew-Burke-Ernzerhof (PBE) [58] functional and the projector augmented-wave (PAW) pseudopotential [59]. The energy cutoff is set to 400 eV for the plane-wave basis and BZ integration was performed on a regular mesh of $8 \times 8 \times 8$ k points. The band structure here is also checked by nonlocal Heyd-Scuseria-Ernzerhof (HSE06) hybrid functional calculations.

*yurui1983@foxmail.com
†hmweng@iphy.ac.cn

TABLE I. Crystallographic data for CaP_3, $CaAs_3$, SrP_3, $SrAs_3$, and $BaAs_3$.

Formula	CaP_3 [54]	$CaAs_3$ [55]	SrP_3 [56]	$SrAs_3$ [57]	$BaAs_3$ [55]
Space group	$P\bar{1}$	$P\bar{1}$	$C2/m$	$C2/m$	$C2/m$
a (nm)	0.5590	0.5866	0.58681	0.61353	0.6393
b (nm)	0.5618	0.5838	0.5690	0.588	0.6015
c (nm)	0.5665	0.5921	0.58681	0.61353	0.6393
α (deg)	69.96	70.04	71.825	72.257	71.485
β (deg)	79.49	80.16	76.777	76.897	74.733
γ (deg)	74.78	75.85	71.825	72.257	71.485

A tight-binding model based on the maximally localized Wannier functions (MLWFs) [60,61] of the p orbits of P or As has been constructed in order to investigate the surface states of the (001) surface.

III. RESULTS AND DISCUSSION

A. Electronic structure

The band structures of the CaP_3 family of materials are presented in Fig. 2 without spin-orbit coupling (SOC). The result of the GGA-PBE calculation shows that two bands with opposite parity are inverted around the Y point near the Fermi energy. In addition, the symmetry at the Y point is composed of time reversal symmetry (TRS) and space inversion symmetry (SIS) for the $P\bar{1}$ symmetry materials, and for the $C2/m$ symmetry materials, there is an additional symmetry, the mirror symmetry (MS). As proposed in our early work, in the case of the coexistence of time reversal symmetry and space inversion symmetry, the energy inverted bands with opposite parity should cross along a closed nodal line [27,32,44]. The nodal line structures are located at the Γ-Y-S plane for SrP_3, $SrAs_3$, and $BaAs_3$, as shown in Figs. 2(a)

TABLE II. Atomic coordinates, and equivalent isotropic displacement parameters for CaP_3, $CaAs_3$, SrP_3, $SrAs_3$, and $BaAs_3$.

Atoms	Site	Wyckoff symbol	x	y	z
CaP_3	Ca	$2i$	0.175	0.141	0.146
	P1	$2i$	0.498	0.303	0.501
	P2	$2i$	0.630	0.320	0.104
	P3	$2i$	0.104	0.300	0.600
$CaAs_3$	Ca	$2i$	0.1847	0.1595	0.1243
	As1	$2i$	0.5104	0.2829	0.5149
	As2	$2i$	0.6449	0.3130	0.0928
	As3	$2i$	0.0895	0.2801	0.5907
SrP_3	Sr	$2i$	0.1618	0.1477	0.1618
	P1	$2i$	0.6156	0.3205	0.1036
	P2	$2i$	0.4895	0.3094	0.4895
$SrAs_3$	Sr	$2i$	0.1631	0.1655	0.1631
	As1	$2i$	0.6291	0.3054	0.0939
	As2	$2i$	0.5040	0.2878	0.5040
$BaAs_3$	Ba	$2i$	0.1637	0.1630	0.1637
	As1	$2i$	0.6272	0.3165	0.0956
	As2	$2i$	0.4958	0.2969	0.4958
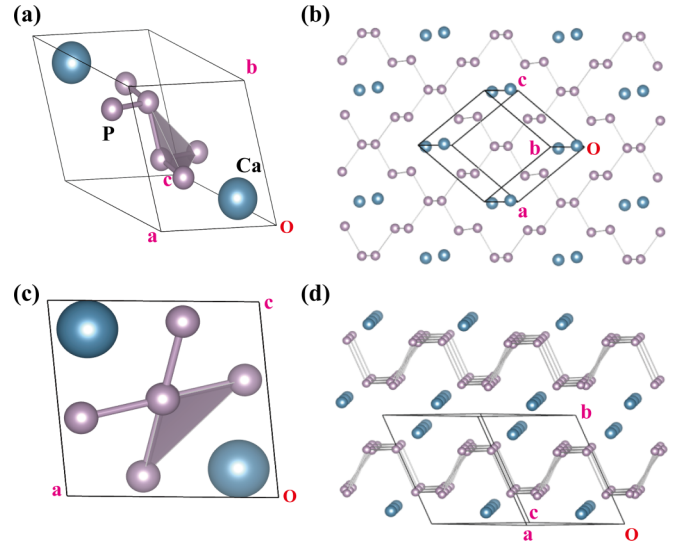
FIG. 1. (a) is the primitive cell of CaP_3. The side view of the primitive cell along the b axis is shown in (c). (b) is the top view of a single layer of CaP_3. The puckered P layers (gray colored balls) can be derived from orthorhombic black phosphorus by removing 1/4 of the P atoms. (d) is the side view of the crystal structure of CaP_3. The puckered polyanionic layers stack along the b axis.

and 2(b), while for CaP_3 and $CaAs_3$ the nodal line is slightly deviated from this plane.

We have performed the HSE06 calculation to check the band structures near the Y point, which are shown by the red dotted curves in Figs. 2(c)–2(g). We find that only $SrAs_3$ shows a band inverted structure in the HSE06 calculation, while the bands of the other four compounds are in normal order. Therefore, the nodal line structure survives in $SrAs_3$, but vanishes in the other four materials. On the other hand, we also find that compressing the lattice volume helps the band inversion to emerge. The band structures of a compressed lattice with the HSE06 calculation are shown as blue dashed curves in Figs. 2(c), 2(d), 2(e), and 2(g). Therefore, compressing the volume can control the emergence of the nodal lines in CaP_3, $CaAs_3$, SrP_3, and $BaAs_3$. Moreover, we also checked that the nonmagnetic phases of these materials are more energetically stable than the magnetic phases.

According to the bulk boundary correspondence, the nontrivial surface states are expected to appear on the surface of the materials. In order to calculate such surface states, we make a detailed analysis of the band structure. The density of states calculation [Fig. 2(h)] and the "fat" band structure [Fig. 2(i)] show that the nodal line structures are mainly composed of $p_x + p_z$ and p_y orbits of P or As atoms. The tight-binding Hamiltonians in the basis of the p orbits of P or As atoms can be obtained by using the MLWF method [60,61], and the surface states for a semi-infinite slab along the c direction can be calculated by using these Hamiltonians. The obtained surface states are nestled between two solid Dirac cones, as shown in Figs. 3(b)–3(f), which are the projections of the nodal line circles in the c direction. Moreover, we find that the surface states also exist in compressed structures [Figs. 3(g)–3(i)]. The topological nodal line structure is stable when compressing the volume, despite the appearance of another Fermi surface. Here,
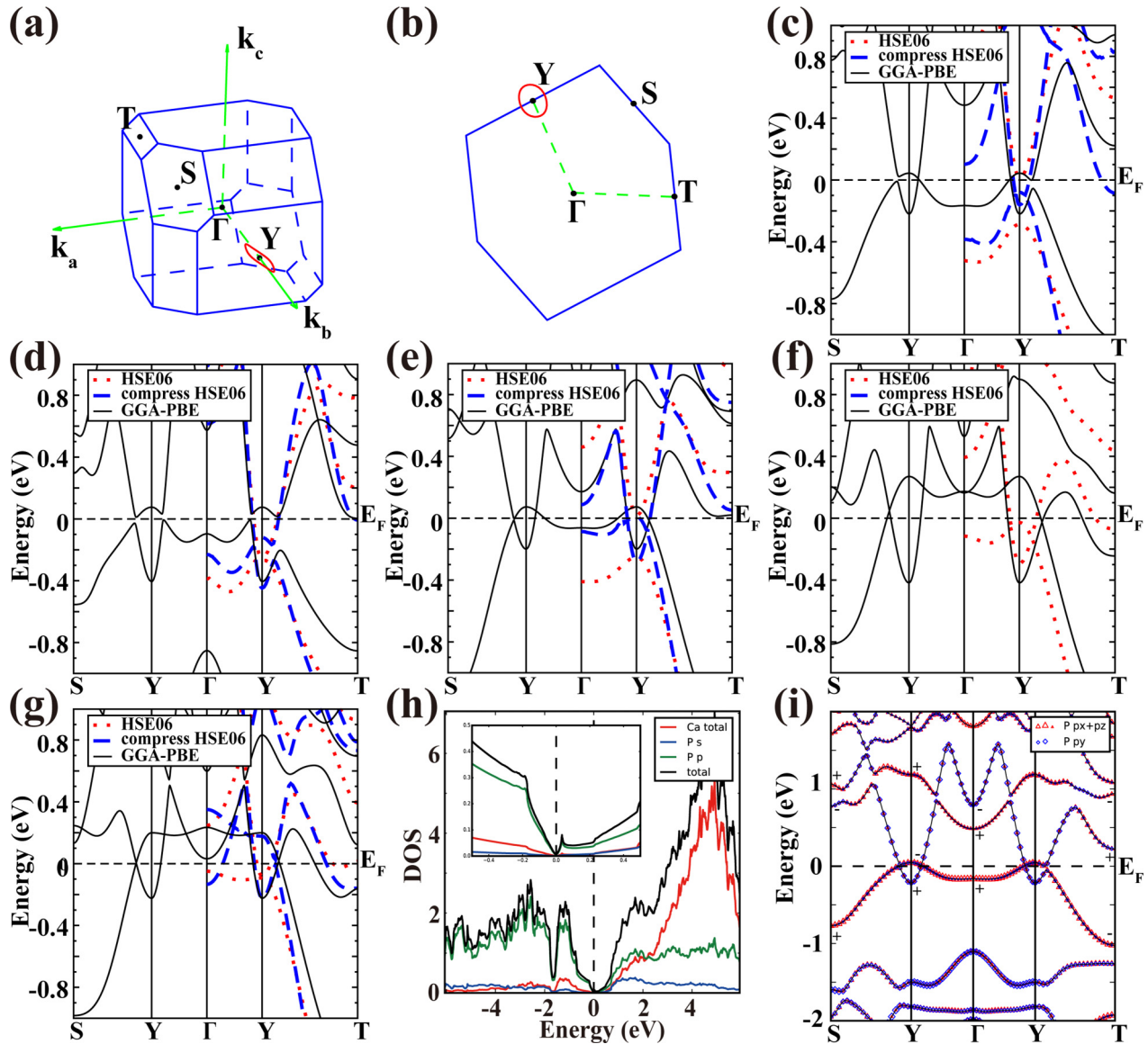
FIG. 2. (a) is the bulk BZ for the CaP$_3$ family of materials. The nodal line (red colored loop) surrounds the Y point and lies on the Γ-Y-S plane for the SrP$_3$, SrAs$_3$, and BaAs$_3$ compounds, while it slightly deviates from this plane for CaP$_3$ and CaAs$_3$. The projection of the nodal line on the Γ-Y-S plane is shown in (b). The band structures from the GGA-PBE calculations are shown as black solid curves for (c) CaP$_3$, (d) CaAs$_3$, (e) SrP$_3$, (f) SrAs$_3$, and (g) BaAs$_3$. The red dotted curves are the HSE06 calculation results and the blue dashed curves are the HSE06 calculation results with a compressed lattice structure $0.94a \times 0.94b \times 0.94c$. (h) is the density of states for CaP$_3$. The p orbits of P (green line) dominate the states around the Fermi energy. (i) The "fat" band structure shows that the nodal line is mainly composed of $p_x + p_z$ (red circle) and p_y (blue circle) orbits of P atoms in CaP$_3$.

we also study the effect of a surface potential on the surface state. We change the on-site energy of the surface atoms of CaP$_3$ to 112%, 120%, and 133% of the pristine value (Fig. 4), and find that the surface state remains inside the nodal line circle, but it will be pushed into the bulk states as the surface potential increases.

In the above calculations, SOC is ignored, and the nodal line structure can be found in BZ. If we take SOC into consideration, gaps will be opened along the nodal line, and these materials become small gap insulators. The gap values along the S-Y and Y-Γ directions are listed in Table III. Since the materials listed have an inversion center, we calculate the production of the parities of the occupied states at the eight time

reversal invariant momenta (TRIM) as listed in Table IV, which indicate that these materials are strong topological insulators with a Z_2 index as (1; 010) [62,63]. The (001) surface states of SrP$_3$ with the SOC having been taken into consideration are shown in Fig. 5(b).

B. Model Hamiltonian

In this section we investigate the nodal line structure from the continuous $k \cdot p$ model. First, we construct the $k \cdot p$ model near the band inversion point from the symmetry principles. Then we calculate the energy dispersions of the surface states by using the obtained $k \cdot p$ Hamiltonian.
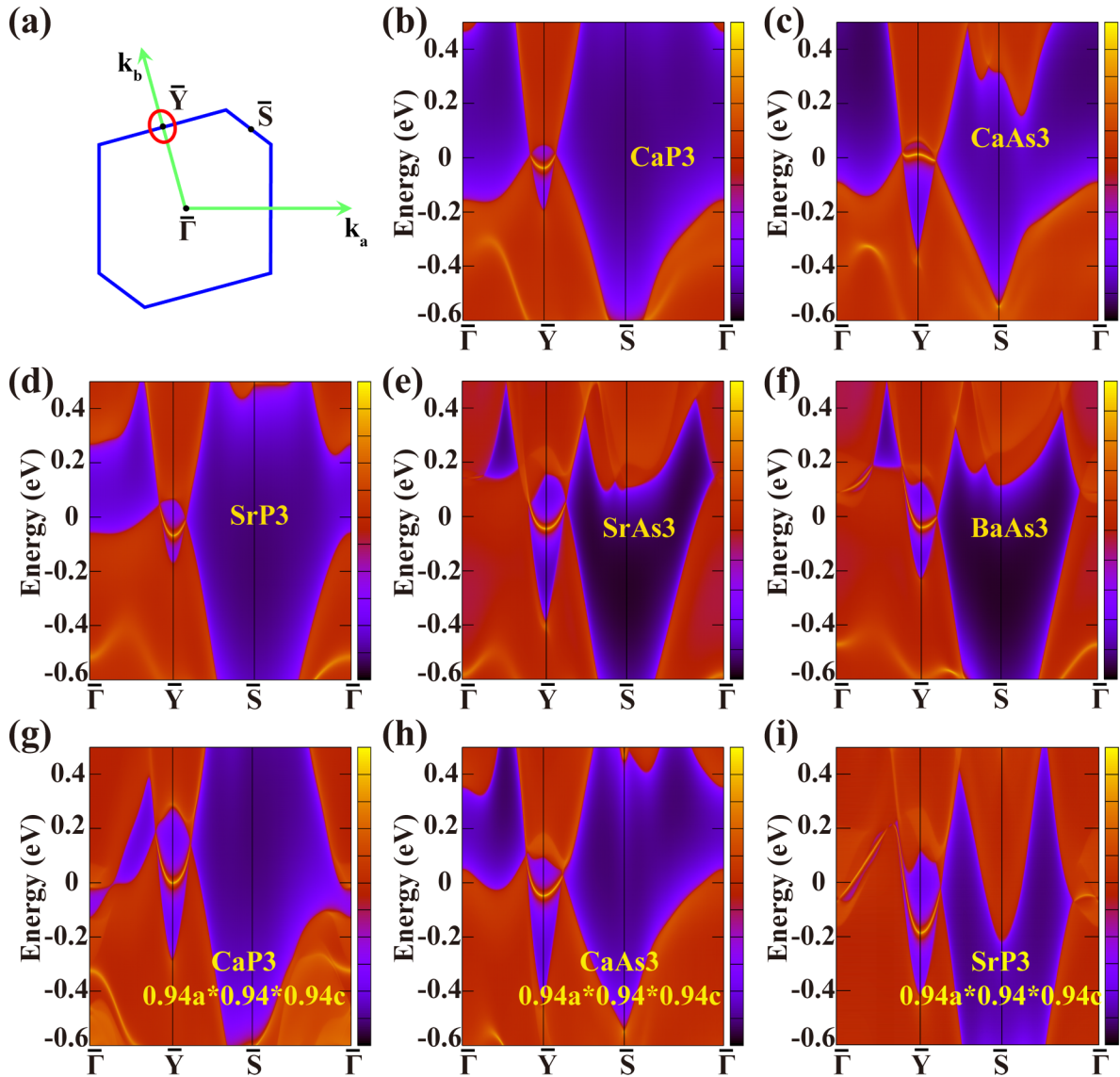
FIG. 3. (a) The projected BZ along the c direction. The surface states (red colored curve near the Y point) for (b) CaP$_3$, (c) CaAs$_3$, (d) SrP$_3$, (e) SrAs$_3$, and (f) BaAs$_3$ are nestled between two solid Dirac cones, which are the projections of the nodal line circles. The (001) surface states of (g) CaP$_3$, (h) CaAs$_3$, and (i) SrP$_3$ with a compressed lattice $0.94a \times 0.94b \times 0.94c$ are also calculated.
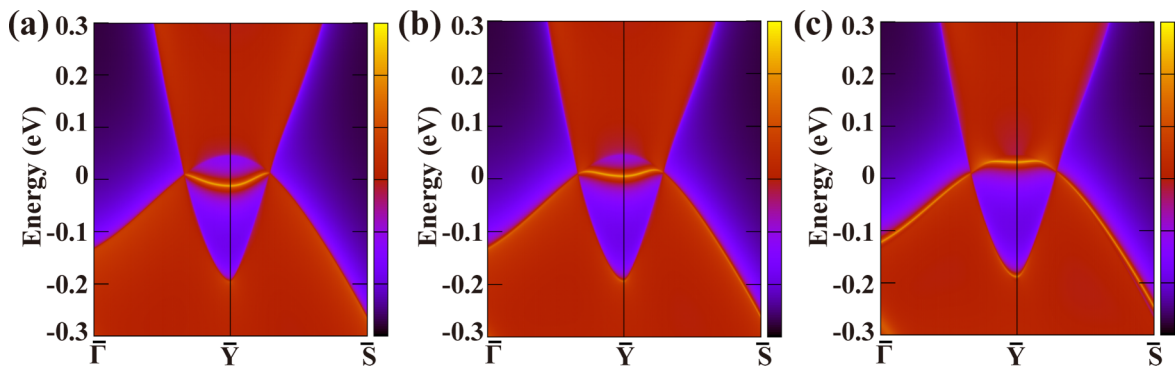
FIG. 4. The surface states of CaP$_3$ as a function of the surface potential. The on-site energy of the surface atoms is changed to (a) 112%, (b) 120%, and (c) 133% of the pristine value.

TABLE III. The gap values near the nodal line after considering the SOC.

	S-Y (meV)	Y-Γ (meV)
CaP_3	31.69	3.73
$CaAs_3$	54.47	39.92
SrP_3	6.11	1.76
$SrAs_3$	47.14	6.28
$BaAs_3$	38.97	6.22

TABLE IV. The parity productions for the occupied states at the TRIM points.

$\Gamma(0,0,0)$	$X(\frac{1}{2},0,0)$	$Y(0,\frac{1}{2},0)$	$Z(0,0,\frac{1}{2})$
−	−	−	−
$(\frac{1}{2},\frac{1}{2},0)$	$(0,\frac{1}{2},\frac{1}{2})$	$T(\frac{1}{2},0,\frac{1}{2})$	$S(\frac{1}{2},\frac{1}{2},\frac{1}{2})$
+	+	−	+

The most general form of a two-band model can be written as

$$H(\mathbf{k}) = \sum_{i=0}^{3} g_i(\mathbf{k})\sigma_i, \qquad (1)$$

where $g_i(\mathbf{k})$ are real functions of $\mathbf{k}$, σ_0 is the identity matrix, and $\sigma_{1,2,3}$ are Pauli matrices for the space which is expanded by the two investigated bands near the Fermi energy. At the band inversion point Y, the symmetry group is reduced to C_i for the $P\bar{1}$ space group materials and $C2h$ for the $C2/m$ space group materials.

The C_i group contains time reversal symmetry $\hat{T}$ and space inversion symmetry $\hat{P}$. For the $C2h$ group, there is an additional symmetry, a mirror symmetry $M : k_a \leftrightarrow k_c; k_b \rightarrow k_b$. At the Y point, the two inverted bands have opposite parity and then the inversion operator can be chosen as $\hat{P} = \sigma_z$. The inversion symmetry constrains the Hamiltonian, satisfying

$$\hat{P} H(\mathbf{k}) \hat{P}^{-1} = H(-\mathbf{k}), \qquad (2)$$

which leads to $g_{0,3}(\mathbf{k})$ being even functions of $\mathbf{k}$ and $g_{1,2}(\mathbf{k})$ are odd functions of $\mathbf{k}$. On the other hand, the time reversal symmetry requires that

$$\hat{T} H(\mathbf{k}) \hat{T}^{-1} = H(-\mathbf{k}), \qquad (3)$$

where $\hat{T} = K$ and K is the complex conjugate operator for the spinless case. The requirement leads to $g_{0,1,3}(\mathbf{k})$ being even functions and $g_2(\mathbf{k})$ are an odd functions of $\mathbf{k}$. Combining

the constraints to $g_i(\mathbf{k})$ from time reversal and space inversion symmetry, we obtain that $g_1(\mathbf{k}) = 0$, $g_{0,3}(\mathbf{k})$ are even functions of $\mathbf{k}$ and $g_2(\mathbf{k})$ is an odd function of $\mathbf{k}$. Keeping up to the lowest order of $\mathbf{k}$, we get

$$g_0(\mathbf{k}) = a_0 + a_1 k_a^2 + a_2 k_b^2 + a_3 k_c^2,$$
$$g_2(\mathbf{k}) = \alpha k_a + \beta k_b + \gamma k_c,$$
$$g_3(\mathbf{k}) = m_0 + m_1 k_a^2 + m_2 k_b^2 + m_3 k_c^2. \qquad (4)$$

For simplicity, the basis vectors in $\mathbf{k}$ space are chosen as k_a, k_b, and k_c, as shown in Figs. 2(a) and 2(b). For the $P\bar{1}$ space group materials CaP_3 and $CaAs_3$, the parameters in Eq. (1) are independent. For the $C2/m$ space group materials, the mirror symmetry can be chosen as $\hat{M} = \sigma_z$, and the mirror symmetry gives an additional constraint to Hamiltonian Eq. (1),

$$\hat{M} H(k_a, k_b, k_c) \hat{M}^{-1} = H(k_c, k_b, k_a), \qquad (5)$$

which reduces the number of parameters by requiring that $\beta = 0$, $a_1 = a_3$, $m_1 = m_3$, and $\alpha = -\gamma$ in Eq. (4).

The $k \cdot p$ parameters obtained by fitting with the first-principle calculations are listed in Table V. The band structures calculated by the $k \cdot p$ model Hamiltonian are compared with the first-principles calculations as shown in Fig. 6

The eigenvalues of Eq. (1) are $E(\mathbf{k}) = g_0(\mathbf{k}) \pm \sqrt{g_2^2(\mathbf{k}) + g_3^2(\mathbf{k})}$ and the band crossing points appear when $g_2(\mathbf{k}) = 0$ and $g_3(\mathbf{k}) = 0$. In the band inversion case, we obtain that $m_0 < 0$ and $m_i > 0$, $i = 1,2,3$. Then, $g_3(\mathbf{k}) = m_0 + m_1 k_a^2 + m_2 k_b^2 + m_3 k_c^2 = 0$ is just an equation for an ellipsoidal surface which surrounds the Y point in $\mathbf{k}$ space. The second condition $g_2(\mathbf{k}) = \alpha k_a + \beta k_b + \gamma k_c = 0$ determines
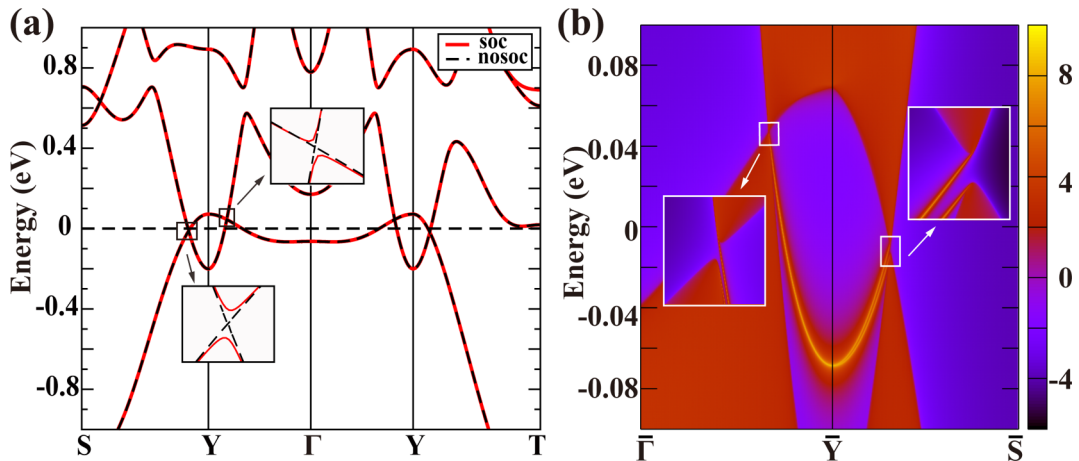
FIG. 5. (a) The band structure of SrP_3 obtained from the GGA-PBE calculation with (red lines) and without SOC (black lines). (b) shows the (001) surface states of SrP_3 with SOC.

TABLE V. The parameters for the $k \cdot p$ Hamiltonian in Eqs. (1) and (4). The unit of energy is in eV and the unit of length is in lattice parameters.

CaP$_3$	a_0	a_1	a_2	a_3	m_0	m_1	m_2	m_3	α	β	γ
	-0.091	1.671	14.372	2.394	-0.142	10.438	19.138	11.910	1.773	0.001	-2.096
CaAs$_3$	a_0	a_1	a_2	a_3	m_0	m_1	m_2	m_3	α	β	γ
	-0.179	1.295	17.702	1.813	-0.240	9.319	23.204	10.578	1.303	0.272	-1.758
SrP$_3$	a_0	a_1	a_2	m_0	m_1	m_2	α				
	-0.095	-2.324	13.619	-0.1167	10.451	17.049	2.156				
SrAs$_3$	a_0	a_1	a_2	m_0	m_1	m_2	α				
	-0.005	-1.778	17.249	-0.3439	12.728	20.989	1.980				
BaAs$_3$	a_0	a_1	a_2	m_0	m_1	m_2	α				
	-0.112	-3.193	15.896	-0.212	11.089	16.5431	1.918				
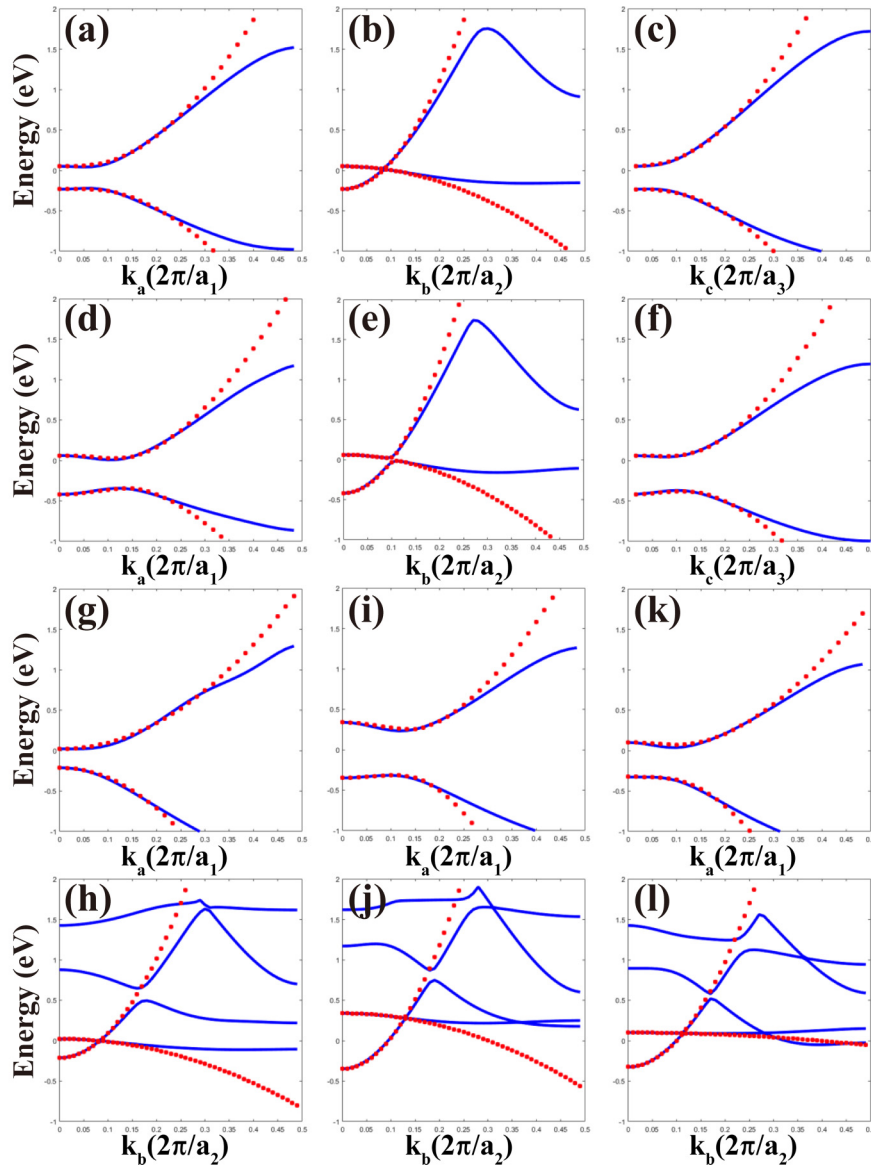
FIG. 6. Comparison of band structures of GGA (blue solid curves) and $k \cdot p$ model (red dashed curves) calculations for (a)–(c) CaP$_3$, (d)–(f) CaAs$_3$, (g), (h) SrP$_3$, (i), (j) SrAs$_3$, and (k), (l) BaAs$_3$.

a plane passing the Y point and with its normal direction along the (α,β,γ) direction. The crossing points between the plane determined by $g_2(\boldsymbol{k}) = 0$ and the ellipsoidal surface determined by $g_3(\boldsymbol{k}) = 0$ form a closed loop, which is just the band closing nodal line between the two inverted bands. For the $C2/m$ space group, where $\beta = 0$ and $\alpha = -\gamma$, the nodal line is located at the plane that passes through k_b and the angular bisector of k_a and k_c exactly. The higher-order terms, such as the fourth-order terms in $g_{0,3}(\boldsymbol{k})$ and the third-order terms in $g_2(\boldsymbol{k})$, will deform the ellipsoidal surface and bend the plane, nevertheless, the crossing nodal line will not disappear but will change to a three-dimensional closed loop as shown in Fig. 1(a).

In the following, starting from the $k \cdot p$ model in Eqs. (1) and (4), we present the solutions for the energy spectra of the surface states of the CaP$_3$ family of materials. As shown in Fig. 1(b), we consider a surface terminated in the c direction. In this case, k_c is perpendicular to the surface and $k_{a,b}$ are parallel to the surface. Following the method proposed in Ref. [64], the Dirac Hamiltonian in Eq. (1) can be written as

$$H(k_a,k_b,k_c) = g_0(\boldsymbol{k}) + \boldsymbol{h}(\boldsymbol{k}) \cdot \boldsymbol{\sigma}, \qquad (6)$$

where $\boldsymbol{\sigma} = (\sigma_1,\sigma_2,\sigma_3)$,

$$\boldsymbol{h}(\boldsymbol{k}) = \boldsymbol{c}^0(k_a,k_b) + \boldsymbol{c}^1(k_a,k_b)k_c + \boldsymbol{c}^2(k_a,k_b)k_c^2, \qquad (7)$$

and

$$\boldsymbol{c}^0 = \left(0, \alpha k_a + \beta k_b, m_0 + m_1 k_a^2 + m_2 k_b^2\right),$$
$$\boldsymbol{c}^1 = (0,\gamma,0),$$
$$\boldsymbol{c}^2 = (0,0,m_3). \qquad (8)$$

The behavior of $\boldsymbol{h}(\boldsymbol{k})$ completely determines the topological nature of the system and it is the key to understanding the relation between the existence of surface states and bulk topological properties. By tuning k_c, the vector $\boldsymbol{h}(\boldsymbol{k})$ forms a parabola in the 2D plane spanned by $\boldsymbol{c}^1$ and $\boldsymbol{c}^2$. As proved in Ref. [64], for the continuum Hamiltonian $\boldsymbol{h}(\boldsymbol{k})$, the surface states exist if the origin is within the concave side of the parabola, which leads to the following equation for k_a and k_b,

$$(\alpha k_a + \beta k_b)^2 + \frac{\gamma^2}{m_3}\left(m_0 + m_1 k_a^2 + m_2 k_b^2\right) < 0. \qquad (9)$$

The energy of the surface states (located on the surface of a semi-infinite slab with $r_c \geqslant 0$) can then be calculated as

$$E_s = \boldsymbol{c}^0 \cdot \frac{\boldsymbol{c}^1 \times \boldsymbol{c}^2}{|\boldsymbol{c}^1 \times \boldsymbol{c}^2|}. \qquad (10)$$

As expressed in Eq. (8), $\boldsymbol{c}^0$ is in the plane spanned by vectors $\boldsymbol{c}^1$ and $\boldsymbol{c}^2$, therefore $\boldsymbol{c}^0$ is perpendicular to $\boldsymbol{c}^1 \times \boldsymbol{c}^2$, which leads to $E_s = 0$. This result indicates that a dispersionless state can exist on the surface of a nodal line semimetal within the area determined by Eq. (9), whereas the topological trivial term $g_0(\boldsymbol{k})$ in Eq. (6) will introduce a finite dispersion and finally lead to drumheadlike surface states as shown in Fig. 3.

IV. CONCLUSION

In summary, we propose that 3D topological nodal line semimetal states can be realized in the CaP$_3$ family of materials when we ignore SOC. A closed nodal line is found near the Fermi energy, and this is protected by time reversal and inversion symmetry with an inverted band in the bulk band structure. The 2D drumheadlike surface states nested inside the closed nodal line are studied in the c direction by using the tight-binding method and a $k \cdot p$ model analysis. Its nearly flat energy dispersion is an ideal playground for many interaction-induced nontrivial states, such as fractional topological insulators and high-temperature superconductivity. After taking the SOC into consideration, the CaP$_3$ family of materials becomes a strong topological insulator with a small energy gap.

[1] H. Weng, X. Dai, and Z. Fang, J. Phys.: Condens. Matter **28**, 303001 (2016).

[2] G. E. Volovik, *The Universe in a Helium Droplet* (Oxford University Press, Oxford, U.K., 2009).

[3] Z. Fang, N. Nagaosa, K. S. Takahashi, A. Asamitsu, R. Mathieu, T. Ogasawara, H. Yamada, M. Kawasaki, Y. Tokura, and K. Terakura, Science **302**, 92 (2003).

[4] H. Weng, R. Yu, X. Hu, X. Dai, and Z. Fang, Adv. Phys. **64**, 227 (2015).

[5] Z. Wang, Y. Sun, X.-Q. Chen, C. Franchini, G. Xu, H. Weng, X. Dai, and Z. Fang, Phys. Rev. B **85**, 195320 (2012).

[6] Z. Wang, H. Weng, Q. Wu, X. Dai, and Z. Fang, Phys. Rev. B **88**, 125427 (2013).

[7] B.-J. Yang and N. Nagaosa, Nat. Commun. **5**, 4898 (2014).

[8] A. Pariari, P. Dutta, and P. Mandal, Phys. Rev. B **91**, 155139 (2015).

[9] L. P. He, X. C. Hong, J. K. Dong, J. Pan, Z. Zhang, J. Zhang, and S. Y. Li, Phys. Rev. Lett. **113**, 246402 (2014).

[10] M. Neupane, S.-Y. Xu, R. Sankar, N. Alidoust, G. Bian, C. Liu, I. Belopolski, T.-R. Chang, H.-T. Jeng, H. Lin, A. Bansil, F. Chou, and M. Z. Hasan, Nat. Commun. **5**, 3786 (2014).

[11] Z. K. Liu, B. Zhou, Y. Zhang, Z. J. Wang, H. M. Weng, D. Prabhakaran, S.-K. Mo, Z. X. Shen, Z. Fang, X. Dai, Z. Hussain, and Y. L. Chen, Science **343**, 864 (2014).

[12] Z. K. Liu, J. Jiang, B. Zhou, Z. J. Wang, Y. Zhang, H. M. Weng, D. Prabhakaran, S. K. Mo, H. Peng, P. Dudin, T. Kim, M. Hoesch, Z. Fang, X. Dai, Z. X. Shen, D. L. Feng, Z. Hussain, and Y. L. Chen, Nat. Mater. **13**, 677 (2014).

[13] H. Weng, C. Fang, Z. Fang, B. A. Bernevig, and X. Dai, Phys. Rev. X **5**, 011029 (2015).

[14] S.-M. Huang, S.-Y. Xu, I. Belopolski, C.-C. Lee, G. Chang, B. Wang, N. Alidoust, G. Bian, M. Neupane, C. Zhang, S. Jia, A. Bansil, H. Lin, and M. Z. Hasan, Nat. Commun. **6**, 7373 (2015).

[15] A. A. Soluyanov, D. Gresch, Z. Wang, Q. S. Wu, and M. Troyer, Nature (London) **527**, 495 (2015).

[16] B. Q. Lv, H. M. Weng, B. B. Fu, X. P. Wang, H. Miao, J. Ma, P. Richard, X. C. Huang, L. X. Zhao, G. F. Chen, Z. Fang, X. Dai, T. Qian, and H. Ding, Phys. Rev. X **5**, 031013 (2015).

[17] X. Huang, L. Zhao, Y. Long, P. Wang, D. Chen, Z. Yang, H. Liang, M. Xue, H. Weng, Z. Fang, X. Dai, and G. Chen, Phys. Rev. X **5**, 031023 (2015).

[18] B. Q. Lv, N. Xu, H. M. Weng, J. Z. Ma, P. Richard, X. C. Huang, L. X. Zhao, G. F. Chen, C. E. Matt, F. Bisti, V. N. Strocov, J. Mesot, Z. Fang, X. Dai, T. Qian, M. Shi, and H. Ding, Nat. Phys. **11**, 724 (2015).

[19] S.-Y. Xu, I. Belopolski, N. Alidoust, M. Neupane, G. Bian, C. Zhang, R. Sankar, G. Chang, Z. Yuan, C.-C. Lee, S.-M. Huang, H. Zheng, J. Ma, D. S. Sanchez, B. Wang, A. Bansil, F. Chou, P. P. Shibayev, H. Lin, S. Jia, and M. Z. Hasan, Science **349**, 613 (2015).

[20] N. Xu, H. M. Weng, B. Q. Lv, C. E. Matt, J. Park, F. Bisti, V. N. Strocov, D. Gawryluk, E. Pomjakushina, K. Conder, N. C. Plumb, M. Radovic, G. Autès, O. V. Yazyev, Z. Fang, X. Dai, T. Qian, J. Mesot, H. Ding, and M. Shi, Nat. Commun. **7**, 11006 (2016).

[21] B. Q. Lv, S. Muff, T. Qian, Z. D. Song, S. M. Nie, N. Xu, P. Richard, C. E. Matt, N. C. Plumb, L. X. Zhao, G. F. Chen, Z. Fang, X. Dai, J. H. Dil, J. Mesot, M. Shi, H. M. Weng, and H. Ding, Phys. Rev. Lett. **115**, 217601 (2015).

[22] C.-K. Chiu and A. P. Schnyder, Phys. Rev. B **90**, 205136 (2014).

[23] C. Fang, Y. Chen, H.-Y. Kee, and L. Fu, Phys. Rev. B **92**, 081201 (2015).

[24] T. T. Heikkilä, N. B. Kopnin, and G. E. Volovik, JETP Lett. **94**, 233 (2011).

[25] T. T. Heikkilä and G. E. Volovik, JETP Lett. **93**, 59 (2011).

[26] T. T. Heikkilä and G. E. Volovik, arXiv:1504.05824.

[27] H. Weng, Y. Liang, Q. Xu, R. Yu, Z. Fang, X. Dai, and Y. Kawazoe, Phys. Rev. B **92**, 045108 (2015).

[28] K. Mullen, B. Uchoa, and D. T. Glatzhofer, Phys. Rev. Lett. **115**, 026403 (2015).

[29] L. S. Xie, L. M. Schoop, E. M. Seibel, Q. D. Gibson, W. Xie, and R. J. Cava, APL Mater. **3**, 083602 (2015).

[30] Y.-H. Chan, C.-K. Chiu, M. Y. Chou, and A. P. Schnyder, Phys. Rev. B **93**, 205132 (2016).

[31] M. Zeng, C. Fang, G. Chang, Y.-A. Chen, T. Hsieh, A. Bansil, H. Lin, and L. Fu, arXiv:1504.03492.

[32] R. Yu, H. Weng, Z. Fang, X. Dai, and X. Hu, Phys. Rev. Lett. **115**, 036807 (2015).

[33] Y. Kim, B. J. Wieder, C. L. Kane, and A. M. Rappe, Phys. Rev. Lett. **115**, 036806 (2015).

[34] Y. Chen, Y. Xie, S. A. Yang, H. Pan, F. Zhang, M. L. Cohen, and S. Zhang, Nano Lett. **15**, 6974 (2015).

[35] G. Bian, T.-R. Chang, H. Zheng, S. Velury, S.-Y. Xu, T. Neupert, C.-K. Chiu, S.-M. Huang, D. S. Sanchez, I. Belopolski, N. Alidoust, P.-J. Chen, G. Chang, A. Bansil, H.-T. Jeng, H. Lin, and M. Z. Hasan, Phys. Rev. B **93**, 121113 (2016).

[36] G. Bian, T.-R. Chang, R. Sankar, S.-Y. Xu, H. Zheng, T. Neupert, C.-K. Chiu, S.-M. Huang, G. Chang, I. Belopolski, D. S. Sanchez, M. Neupane, N. Alidoust, C. Liu, B. Wang, C.-C. Lee, H.-T. Jeng, A. Bansil, F. Chou, H. Lin, and M. Zahid Hasan, arXiv:1505.03069.

[37] L. M. Schoop, M. N. Ali, C. Straßer, A. Topp, A. Varykhalov, D. Marchenko, V. Duppel, S. S. P. Parkin, B. V. Lotsch, and C. R. Ast, Nat. Commun. **7**, 11696 (2016).

[38] J.-M. Carter, V. V. Shankar, M. A. Zeb, and H.-Y. Kee, Phys. Rev. B **85**, 115105 (2012).

[39] H.-S. Kim, Y. Chen, and H.-Y. Kee, Phys. Rev. B **91**, 235103 (2015).

[40] J. Liu, D. Kriegner, L. Horak, D. Puggioni, C. Rayan Serrao, R. Chen, D. Yi, C. Frontera, V. Holy, A. Vishwanath, J. M. Rondinelli, X. Marti, and R. Ramesh, Phys. Rev. B **93**, 085118 (2016).

[41] Y. Chen, Y. M. Lu, and H. Y. Kee, Nat. Commun. **6**, 7593 (2015).

[42] A. Yamakage, Y. Yamakawa, Y. Tanaka, and Y. Okamoto, J. Phys. Soc. Jpn. **85**, 013708 (2016).

[43] Q.-F. Liang, J. Zhou, R. Yu, Z. Wang, and H. Weng, Phys. Rev. B **93**, 085427 (2016).

[44] J. Zhao, R. Yu, H. Weng, and Z. Fang, Phys. Rev. B **94**, 195104 (2016).

[45] M. Hirayama, R. Okugawa, T. Miyake, and S. Murakami, arXiv:1602.06501.

[46] Y. Wang and P. Ye, Phys. Rev. B **94**, 075115 (2016).

[47] G. E. Volovik, *Analogue Gravity Phenomenology*, Lecture Notes in Physics Vol. 870 (Springer, Berlin, 2013), p. 343.

[48] J.-W. Rhim and Y. B. Kim, Phys. Rev. B **92**, 045126 (2015).

[49] Y. Huh, E.-G. Moon, and Y. B. Kim, Phys. Rev. B **93**, 035138 (2016).

[50] Z. Yan, P.-W. Huang, and Z. Wang, Phys. Rev. B **93**, 085138 (2016).

[51] N. B. Kopnin, T. T. Heikkilä, and G. E. Volovik, Phys. Rev. B **83**, 220503 (2011).

[52] G. E. Volovik, Phys. Scr. **T164**, 014014 (2015).

[53] T. T. Heikkilä and G. E. Volovik, arXiv:1504.05824.

[54] W. Dahlmann and H. V. Schnering, Naturwissenschaften **60**, 518 (1973).

[55] W. Bauhofer, M. Wittmann, and H. Schnering, J. Phys. Chem. Solids **42**, 687 (1981).

[56] X. Chen, L. Zhu, and S. Yamanaka, J. Solid State Chem. **173**, 449 (2003).

[57] K. Deller and B. Eisenmann, Z. Naturforsch. B **31**, 1550 (1976).

[58] J. P. Perdew, K. Burke, and M. Ernzerhof, Phys. Rev. Lett. **77**, 3865 (1996).

[59] P. E. Blöchl, Phys. Rev. B **50**, 17953 (1994).

[60] A. A. Mostofi, J. R. Yates, Y.-S. Lee, I. Souza, D. Vanderbilt, and N. Marzari, Comput. Phys. Commun. **178**, 685 (2008).

[61] N. Marzari, A. A. Mostofi, J. R. Yates, I. Souza, and D. Vanderbilt, Rev. Mod. Phys. **84**, 1419 (2012).

[62] L. Fu, C. L. Kane, and E. J. Mele, Phys. Rev. Lett. **98**, 106803 (2007).

[63] J. E. Moore and L. Balents, Phys. Rev. B **75**, 121306 (2007).

[64] R. S. K. Mong and V. Shivamoggi, Phys. Rev. B **83**, 125109 (2011).